TURBOMACHINERY & PUMP SYMPOSIA | HOUSTON, TX
DECEMBER 14-16, 2021
SHORT COURSES: DECEMBER 13, 2021

PROTOTYPE TILTING PAD THRUST BEARING WITH NOVEL CERAMIC MATERIAL FOR HARSH SERVICE ENVIRONMENTS

Karel De Raeve
Development Engineer Subsea Pumps
Sulzer Management Ltd
Winterthur, Switzerland

Thomas Kraenzler
Head Global Core Technology Materials
Sulzer Management Ltd
Winterthur, Switzerland

Tiago Borsoi Klein
Professor for Manufacturing Technologies
Beuth University of Applied Sciences Berlin
Berlin, Germany

Andreas Kailer
Group Manager Wear Protection and Advanced Ceramics
Fraunhofer Institute for Mechanics of Materials IWM
Freiburg, Germany

Björn Matthey
Research Associate Fraunhofer Institute
for Ceramic Technologies and Systems IKTS
Dresden, Germany

Steffen Kunze
Research Associate Fraunhofer Institute
for Ceramic Technologies and Systems IKTS
Dresden, Germany

Christian Schmiedel
Research Engineer Fraunhofer Institute
for Production Systems and Design Technology
Berlin, Germany

Stephan Faulhaber
Technical Manager
Miba Industrial Bearings Germany GmbH
Göttingen, Germany

ABSTRACT

Product-lubricated pumping applications require extremely robust bearings, especially in the case of sand-loaded lubrication fluids. For high power/high speed pump applications, tilting pad bearings are the preferred bearing solution, due to their superior rotordynamic characteristics. For product-lubricated applications, materials with good corrosion and abrasion resistance characteristics have to be used. The lubricant for the bearing in these applications is often a water based fluid (e.g. sea water) with low viscosity and with particle contamination (e.g. sand). Existing tilting pad product lubricated bearings (PLB) solutions have the issue that catastrophic failures tend to occur under severe conditions or that they are limited in available size (e.g. polycrystalline diamond (PCD) bearings). A tilting pad thrust bearing and a thrust collar made of a novel ceramic material with improved tribological properties was designed, manufactured and tested for use in such applications.

This new ceramic bearing offers several advantages over existing PLB materials.

- Lower coefficient of friction and reduced start-up torque
- Excellent dry-running capabilities
- Increased reliability and robustness
- Increased wear and abrasion resistance
- No size limitation due to manufacturing constraints such as for PCD bearings

The novel ceramic material is a Diamond-SiC composite, and the material has been tested extensively as per its tribological and wear/erosion characteristics before its use and application in a prototype thrust bearing and thrust collar.

MOTIVATION AND BACKGROUND FOR DEVELOPMENT OF NEW CERAMIC BEARING MATERIAL

Introduction

Water injection is one of the main methods to increase oil recovery and to extend the life of an oil field. It allows maintaining or reducing the decline of the reservoir pressure. The working principle is voidage replacement, namely for each barrel of oil produced from the field, a barrel of water needs to get injected. This injected water flow is called the make-up water. Later in the life of the field, the wells tend to start producing a mixture of oil and water. The produced water together with the make-up water must be reinjected into the field to maintain the reservoir pressure.

For offshore installations, the source for the make-up water is seawater. The seawater needs to go through a water treatment process to make it compatible with the reservoir formation. The typical water treatment and injection process goes through several filtration steps to remove all particles, organic materials, sulfates and oxygen.

The typical filtrations steps consists of a pre-treatment step for the removal of organic material, a micro-filtration step and an ultra-filtration step. For certain oils reservoirs it is required that sulfates are removed from the injection water to avoid scale formation within the reservoir. In this case, there is an additional sulfate removal unit (SRU) having a nano-filtration or a reverse osmosis filtration step.

The water injection pumps need to generate significant pressure rise in order to be able to inject the water into the reservoir. The pressure rise needs to overcome the back-pressure of the reservoir as well as the pressure losses in the flow lines to the injection well heads. The required pressure rise can be as high as 1,000 bar (Üre Villoria & Welschinger, 2014).

Value proposition of a topside product lubricated water injection pump

A conventional water injection pump is equipped with mechanical seals to separate the process fluid from the clean lube oil used to lubricate the bearings. This means that such a unit requires a lube oil system, which consist of a lube oil pump and lube oil cooler. It also needs a seal lubrication system, typically including a circulation pump and a cooler. On top this, such a unit would also need a seal and lube oil storage tank, and which requires periodic replenishment. The mechanical seals are typically of the components in a water injection pump which limit the mean time between maintenance (MTBM).

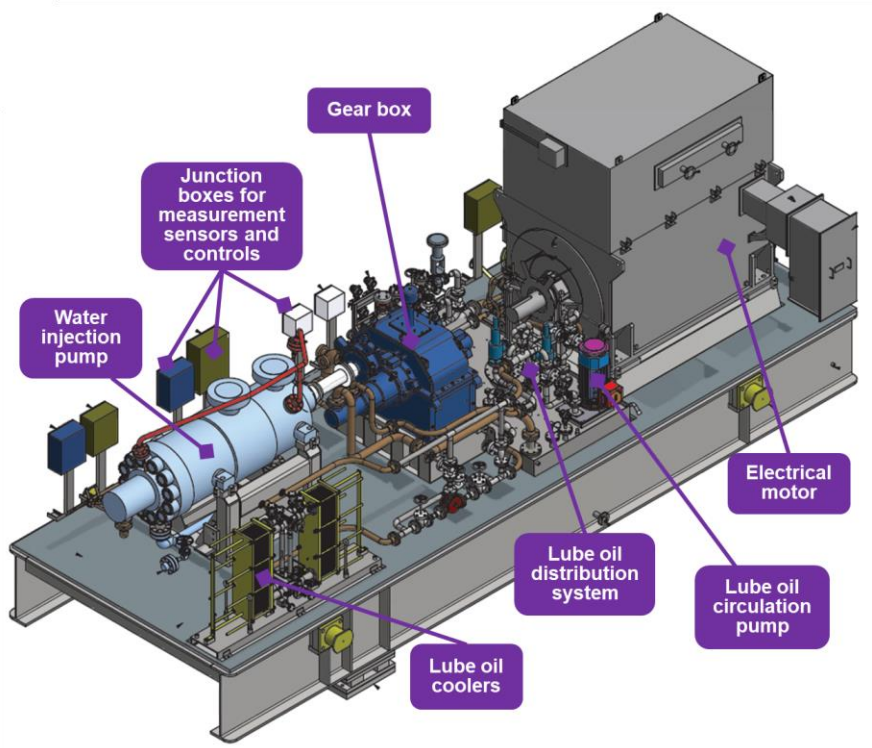

Figure 1: A typical skit of a water injection pump with motor, gearbox and auxiliary systems

Given the above, a process lubricated water injection pump represents a significant simplification of the overall unit since all the auxiliary equipment handling and cooling the seal fluid and lube oil is no longer needed. This represents a significant reduction in capital expenditures (CAPEX) and operating expenditures (OPEX). On top of this, the mechanical seals are therefore also no longer needed, which can present an improvement on the MTBM under the assumption that the product lubricated bearings are reliable.

In the 1990s, Sulzer was a pioneer in the development of product lubricated, high power, water injection pumps (Swann, Watkins, & Bornstein, 1997). Throughout the 1990s a dozen pump units were manufactured with product lubricated bearings, and which allowed

Sulzer to get significant field experience with product lubricated bearings. Unfortunately, a significant amount of failures were observed, and which resulted in the retrofit of several of the pumps back to conventional (oil lubricated) units.

Towards the end of the 1990s, Sulzer came to the conclusion that the bearing technology available on the market at that time for product lubricated applications did not meet the technical requirements in terms of robustness and reliability demanded by the high power and high speed water injection pump applications. By lack of suitable technology, Sulzer decided to discontinue its product offering of product lubricated water injection pumps even though there was a clear market interest for such an offering. The large majority of the bearing failures was related to the thrust bearings. Most of the failures occurred during the start-up from standstill of the pumps.

Figure 2: A failed product lubricated ceramic TPTB.

As can be seen from Figure 2, the failure of a product lubricated bearing tends to be catastrophic. This is due to the nature of the material that is used for the manufacturing of these bearings. The hard materials, which are used for the contact surfaces, are chosen for their excellent erosion/abrasion resistance properties, but have a major drawback because of their brittleness and poor dry-running capability.

Value proposition for a subsea product lubricated water injection pump

Another application for which reliable and robust product lubricated bearings could be a game changer is subsea water treatment and injection, in particular for subsea tie-backs. For a field development with long tie-backs, it is economically more interesting to have the water treatment and injection on the seabed close to the injection well instead of placing it on a platform. For long tie-backs the cost of the high-pressurized injection line can even become a show stopper for a project.

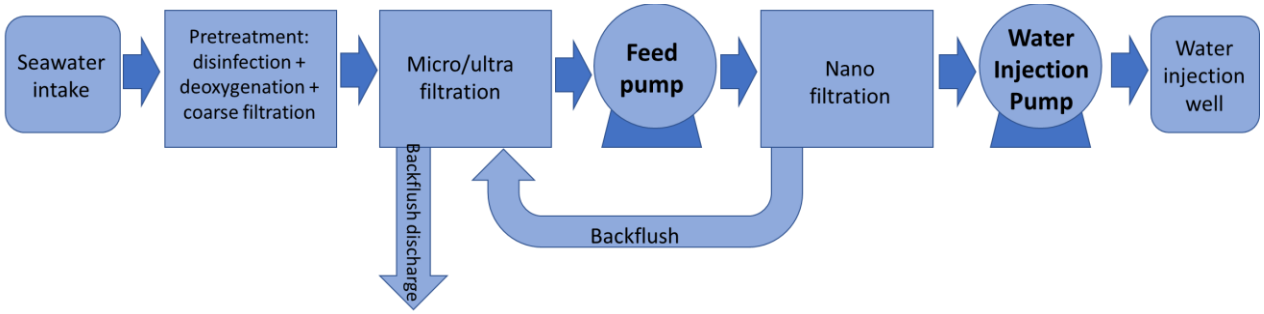

Figure 3: A typical subsea water treatment and injection system. *(Patent No. WO2014206919A1, 2013)*

Lindøen-Kjellnes presented an interesting model framework for the comparison of lifecycle greenhouse gas emissions and business value for topside versus subsea water treatment and injection facilities (Lindøen-Kjellnes, 2021). The impact of parameters such as tie-back distance, water depth as well as installation and modification costs were studied. For longer distances and significant water depths, subsea water treatment and injection is more beneficial in terms of economics and CO_2 emissions.

A hybrid solution consists of having the subsea water injection station close to the well and the water treatment system on the topside. The hybrid solution has the advantage of having a low pressure pipeline from the topside to subsea water injection pump, instead of the high pressure pipeline which is needed for the full-topside solution, as can be seen in Figure 4.

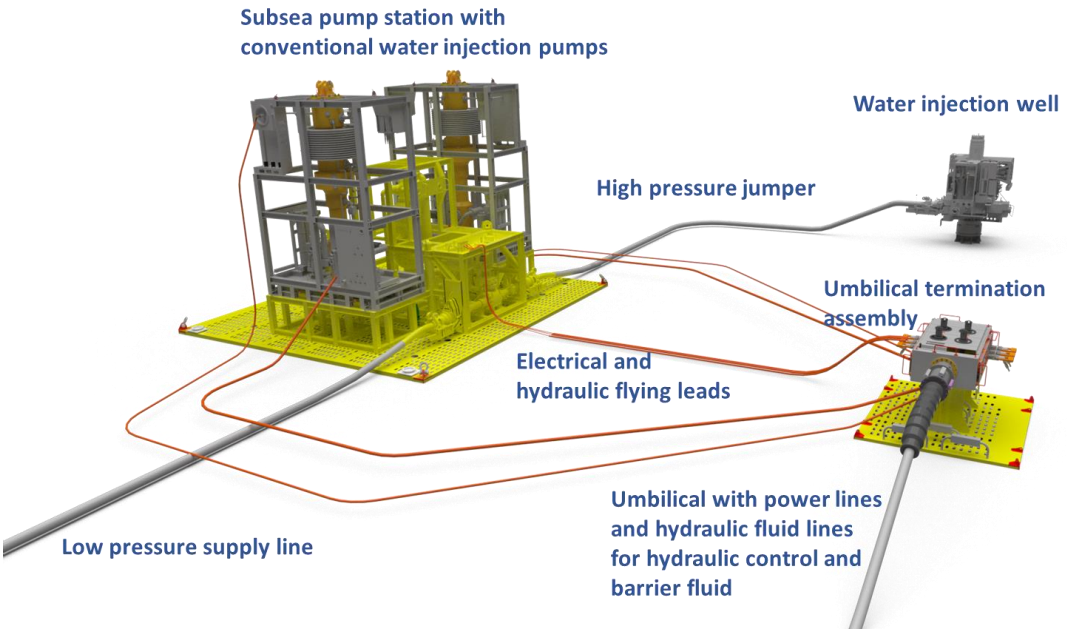

Figure 4: A subsea water injection station with conventional water injection pumps

In a conventional subsea water injection pump, similar to a conventional topside water injection pump, the bearings and the motor compartment are isolated from the process fluid by mechanical seals. The barrier fluid zone within the integrated pump-motor unit is kept at an overpressure relative to the process fluid zone. Hence, during operation, there is a constant leakage of the barrier fluid toward the process fluid and a constant supply of barrier fluid is required.

The barrier fluid is supplied from the topside by a hydraulic pressure unit. The barrier fluid supply lines from the topside to the pump station are bundled together with the power lines in a subsea umbilical. The umbilical arrives at the umbilical termination assembly (UTA), and from which the hydraulic and electrical flying leads are connected to the connection points on the pump station.

A sealless subsea water injection pump would bring some major cost savings. The umbilical is a major CAPEX component of a subsea development. A sealless unit would allow for a replacement of the umbilical with a simple power cable. Note the topside hydraulic power unit (HPU) and the barrier fluid storage are no longer be needed, hence freeing up expensive topside deck space.

Figure 5 shows a sealless subsea pump motor unit. The unit has a 4+4 stages back-to-back configuration. The throttle bush leakage flow (lines) is routed through the bearings and motor for cooling and lubrication. As can be seen such a unit is simpler and lighter than a conventional subsea unit as it dispenses the mechanical seals and the subsea barrier fluid cooler.

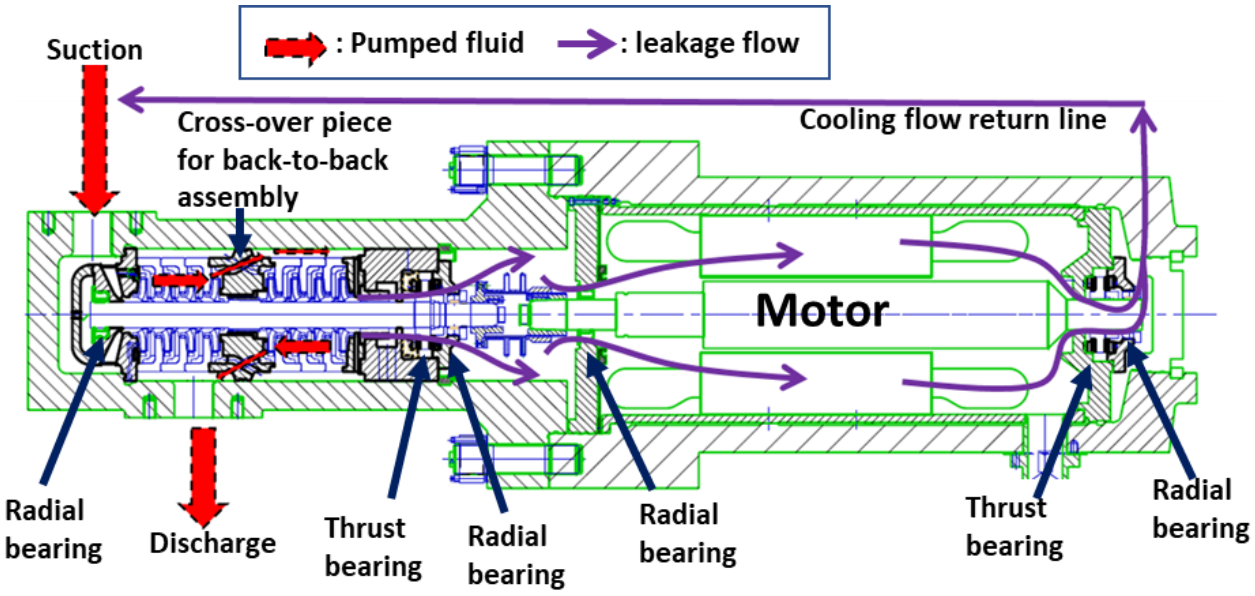

Figure 5: A seal-less product lubricated and cooled subsea water injection pump-motor unit. (Patent No. EP3808984A1, 2019)

Conclusion on the motivation for the technology development

Reliable and robust product lubricated bearings are essential for the successful development of a product lubricated water injection pump. This could be a game changer for both the topside and subsea water injection market in terms of CAPEX and OPEX savings and increased MTBM and thus up-time of the equipment.

Based on Sulzer experience from the 1990s, it is clear that a new product lubricated bearing technology has to be developed for the market. A particular focus of such a development is to produce a reliable and robust thrust bearing capable of (multiple) start-ups under load.

Fraunhofer Society, Miba and Sulzer jointly developed such a prototype tilting pad thrust bearing for product lubricated applications, and which meets the stringent technical requirements. Each partner has brought complementary know-how to the development; namely Sulzer as the rotating equipment specialist, Miba Industrial Bearings Germany (MIBG) as the bearing specialist, and the Fraunhofer Society as the material and manufacturing technology specialist.

OVERVIEW OF THE MATERIALS CURRENTLY USED FOR PRODUCT LUBRICATED BEARINGS

Product lubricated bearings in water injection applications are exposed to harsh conditions. Materials for these components must fulfil certain requirements:

- High strength and toughness to withstand a mechanical load.
- High hardness for wear resistance.
- Low coefficient of friction to reduce heat generation under dry running and starved lubrication conditions.
- High thermal conductivity to dissipate heat caused by lack of lubrication.
- Dry (no lubricant) running capability.

With respect to wear resistance, only ceramics and cermets can guarantee the required lifetime in this environment. Considering the material hardness and thermal conductivity, silicon carbide (SiC) and tungsten carbide (TC) are good candidates. Due to their outstanding corrosion resistance as well as wear resistance, SiC based ceramics are among the most widely used materials for bearings and dynamic seals. Moreover, a low friction coefficient < 0.1 is feasible even under mixed lubrication conditions (Presser, et al., 2009). However, under more severe operation conditions or temporary lack of lubrication, standard SiC materials may show unstable friction behavior, and which limiting the dry running capability often results in catastrophic failure. This is obviously not acceptable for these type of applications where uptime is essential.

The best solution would be pure diamond with its very high hardness, exceptional thermal conductivity, and a low coefficient of friction. However, pure diamond cannot yet be produced in the required dimensions, e.g. for a thrust collar having rings up to 300 mm in diameter. The application of thin CVD (carbon vapor deposition) diamond coatings, known in mechanical seals to improve their dry running capability, brings the risk of delamination under high load operation.

Given the above described limitations, it is clear that a new material is needed which overcomes the shortcomings of the currently available materials for extreme operating conditions.

NEW MATERIAL DEVELOPMENT: MATERIAL CHARACTERISTICS AND MATERIAL TESTS PERFORMED

To fulfill the most demanding requirements and to operate reliable under extremely severe operating conditions, a novel material was engineered, namely a composite SiC-bonded diamond material. This material has unique corrosion (Herrmann, Kluge, Rödel, McKie, & van Staden, 2014) (Matthey, et al., 2017) and wear resistance properties. It maintains its high mechanical strength over extremely long service periods and the friction coefficient remains low and fairly constant under a variety of operating conditions; even in the absence of a lubricating fluid, namely under dry-running conditions.

The new ceramic bonded diamond material can be fabricated using conventional ceramic technologies equal to the preparation of reaction bonded SiC ceramics. So, there is no need of the use of high pressure like in the preparation of polycrystalline diamond composites (PCD). In this way, there are many possibilities in size, shape and complexity for this class of material.

For the application, a mixture of two diamond grain sizes was used, namely 50 µm and 5 µm. The diamond particles were mixed with an organic additive and suspended in a solvent. This suspension is the base for the diamond granulation process, which was performed in a spray dryer to get a diamond granulate for the shaping process. The components were compressed in a uniaxial press, and followed by pyrolysis of the compressed moldings.

During the process, the organic binders are transformed into a glassy carbon by splitting off the volatile compounds. This results in a defined porosity in the pyrolyzed body. In this carbon-bonded state, the material can be processed very easily, for example by CNC milling machines. So, most of the contours of the final components can be machined in this state. The final step is a silicon infiltration above the melting temperature of silicon. ~1420 °C. During the siliconizing process, the liquid silicon flows into the pores of the material.

In the process, the carbon of the pyrolyzed binder as well as some carbon of diamond dissolve in the liquid silicon and forms silicon carbide on the surface of the diamond particles. In the case of a nearly ideal packing of the diamond particles very low contents of residual silicon in the range of less than 3 % in volume can be achieved. Figure 6 depicts pictures of the resulting microstructure.

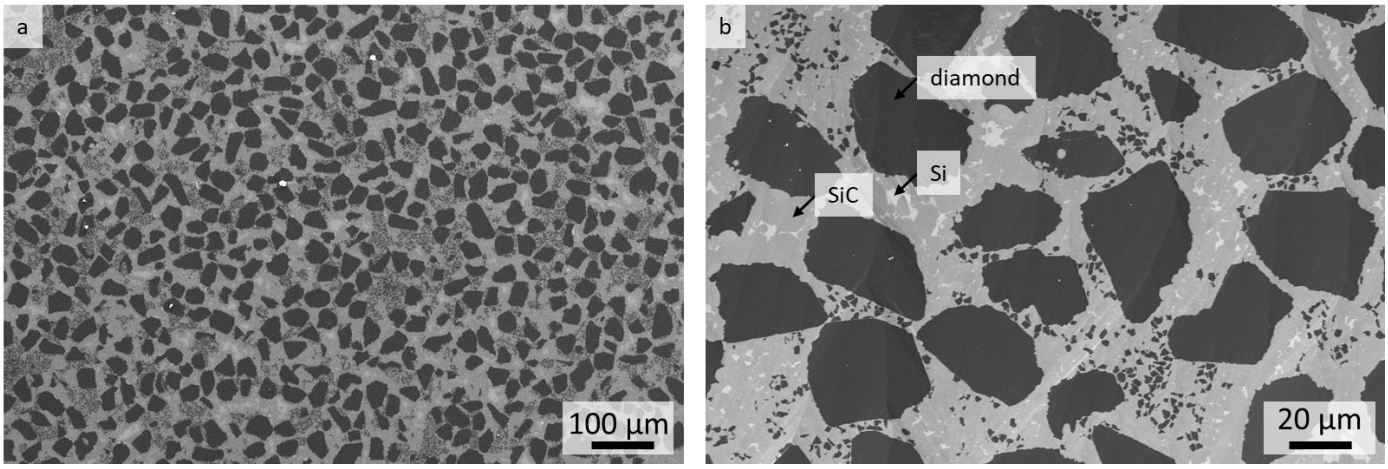

Figure 6: Microstructure of a Diamond-SiC composite (a). The containing phases of diamond (50 µm and 5 µm grain size), silicon carbide and silicon is shown (b).

Besides this preparation of bulk Diamond-SiC composites, it is also possible to prepare layered composites with a substrate layer of conventional silicon infiltrated reaction bonded silicon carbide (Si-SiC) The advantage of this method is the possibility to machine different contours in regions without diamond, which is more cost effective as hard machining of diamond containing regions. Typical features which can be machined in the softer base material are the groove for the metal pivot and the grooves at the side of the pad for the heads of the pad retention bolds. The choice of material variant, whether bulk or graded, depends on size, shape and processing requirements.

The pads, for example, were produced in a graded design, since the various features of the reverse side can be very well represented in Si-SiC and were machined after silicon infiltration process. In the case of the thrust collar the material was a bulk diamond SiC composite. All contours were machined in the carbon bonded preform, and only the finishing process of the surface were machined in the ceramic state. In comparison to silicon infiltrated reaction bonded (Si-SiC) and solid phase sintered (SSiC or simply SiC), Diamond-SiC composites exhibit higher magnitudes for their mechanical properties, see Table 1 which includes comparisons to other commeon materials. The hardness is dependent on the diamond content and shows values up to 49 GPa. The fracture toughness shows a dependency on the residual silicon content. For the material used in this case, values of 4.96 MPa.m$^{0.5}$ were measured. Depending on the surface finish a biaxial strength of around 500-600 MPa was achieved. The thermal conductivity of the composites showed very high magnitudes because of the outstanding thermal conductivity of diamond. The thermal conductivity depends on the diamond content as well as the diamond grain size connected with the amount of grain boundaries. For the used material with a maximum diamond grain size of 50 µm, a thermal conductivity of 450 W/m·K was achieved.

Table 1 Materials properties of a Diamond-SiC composite, Si-SiC, Al_2O_3 and steel.

Materials properties	unit	Diamond-SiC	Si-SiC	Al_2O_3	Steel (S235JR)
Hardness (Vickers)	GPa	49	14-25	17-23	2
Youngs modulus	GPa	525	270-400	280-400	210
Fracture toughness	$MPa \cdot \sqrt{m}$	5	3-5	4	50
Strength	MPa	500-600	180-400	300	370
Coefficient of thermal expansion	$10^{-6}\ 1/K$	4.0	4 - 4.8	7 - 8	11
Thermal conductivity	W/m·K	450	100-160	19-30	50
Resistivity (20°C)	$\Omega \cdot cm$	1,5	$1\ 10^{4}$	$1\ 10^{14}$	0,2

On a model scale, abrasion resistance of Diamond-SiC materials was compared with other materials using an abrasion test according to ASTM G65, in which a rubber or steel wheel is sliding against a sample surface and sand is continuously fed into the sliding contact to induce an abrasive effect. During this test, wear occurred either due to microplastic removal of material or due to brittle surface fatigue.

Figure 7 shows the results of these tests where the depth of the wear profile depth is depicted for several materials. Subsequent surface analyses were made but are not included in this lecture. It is obvious that the Diamond-SiC material achieves the lowest wear profile depth and therefore (by far) the highest resistance to wear. Other materials show higher abrasion rates because of plastic micro ploughing (steel) or severe brittle surface fatigue (Al_2O_3 ceramic).

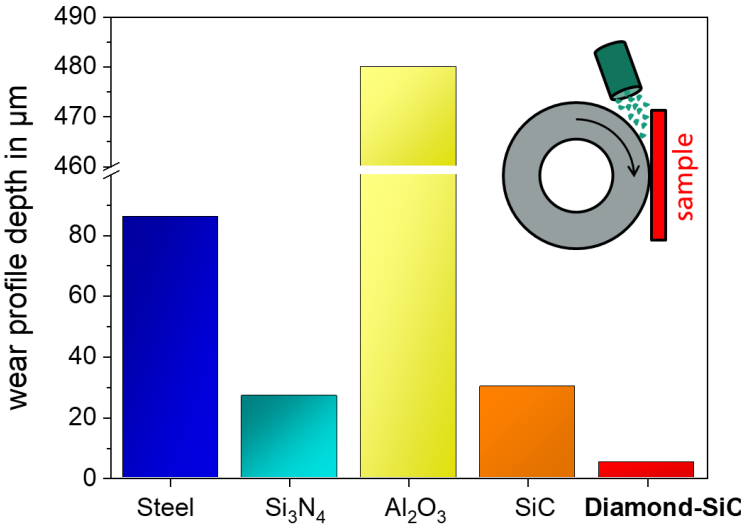

Figure 7: Abrasion resistance for various materials. Tests according to ASTM G65, using a steel wheel and sand particles as abrasive (testing time: 12 min, load: 130 N, quartz sand mean grain size 0.18 mm, sand feeding rate: 120 g/min).

To investigate the tribological behavior of Diamond-SiC ceramics with respect to applications in dynamic (mechanical) seals or slide bearings in an aqueous environment, ring-on-ring tests were conducted under saltwater immersion. Figure 8 shows results for friction coefficients of diamond-SiC and a reference SiC material, commonly used in dynamic mechanical seals (Bernhard, Droescher, Gassmann, & Inforsati, 2016). For all mechanical loads that directly correspond to contact pressures between 0.1 MPa (100 N load) and 0,3 MPa (300 N), the Diamond-SiC material shows significantly lower, steady or constant friction coefficients.

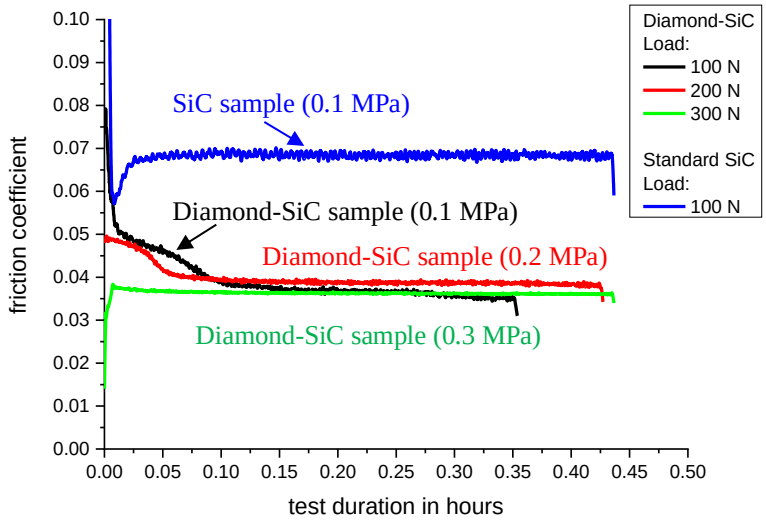

Figure 8: Friction coefficients of Diamond-SiC and a reference SiC ceramic at different loads (contact pressures). Lubrication: Salt water (1 mole per liter), contact pressures: 0.2 MPa, 0.4 MPa and 0.6 MPa (at axial load 100 N, 200 and 300 N, respectively). Sliding velocity: 0.45 m/s. The ring on ring samples are submerged in clean saltwater.

In further tests that started under the same conditions as the test described above, the material was extensively tested to assess its dry running capabilities. The test material went through a high number of cycles consisting of an alternation between water lubricated and dry-running conditions. The sequence of tests was performed with varying conditions such as load, elapsed time duration, lubrication temperature and surface sliding speeds.

Figure 9 shows the final test of the Diamond-SiC material. In this final test, the behavior of the extensively cyclically tested Diamond-SiC sample is compared to the behavior of a pristine sample of SiC. In the test, the water pool was removed after a running-in time of 60 minutes. It is clearly visible that the friction coefficient of the Diamond-SiC combination stays low until the end of the test, while the reference SiC sample almost instantly shows an unstable friction factor behavior; that is, with sudden changes of the friction coefficient, to eventually aborting a test due to a preset friction limit of 0.5. On the other hand, the Diamond-SiC shows a nearly constant friction coefficient even after one hour of dry running. Dry running conditions are abnormal but could occur briefly during start-up of a pump due to an improper start-up procedure.

During the multiple dry running test cycles, it was observed that the friction coefficient marginally increases with each cycle. During the 17 test cycles, the friction coefficient slightly increased from 0.035 to 0.05. This can be explained with almost neglectable changes in the surface state of the material after each dry running test cycle. An example of those changes in surface state is discussed in the section "Detailed analysis of the pad surface after the qualification test". This section discusses the observed changes in micro-topography due to the polishing which occurs under boundary lubrication conditions.

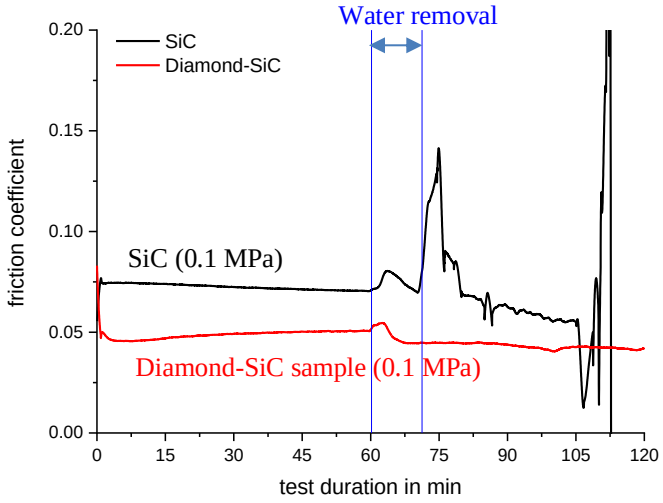

Figure 9: Friction coefficient vs time after removal of water lubrication, contact pressure: 0.1 MPa, sliding velocity: 0.45 m/s

On the basis of the results obtained for the samples tested, one could assert that the friction coefficient for a Diamond-SiC bearing pad will be low and nearly constant under rather severe water-starvation operation conditions, including a temporary dry-running condition. It may be expected that no corrosive material degradation will take place and that these materials and components will be extremely resistant against abrasion by hard particles.

CERAMIC THRUST COLLAR AND TILTING PAD THRUST BEARING DESIGN

The novel Diamond-SiC composite material is used for the manufacturing of components that demand high wear resistance; namely the thrust collar and the tilting pads.

Technical requirements

A typical application for product lubricated bearings is high-speed, high-energy pumps. The demanding technical requirements are:

- Excellent abrasion resistance, well within the range of known polycrystalline diamond (PCD)
- Dry running capability superior to common SiC materials
- Excellent corrosion resistance against seawater, brine and produced water; namely immune against corrosion
- MTBM (mean time between maintenance interval) of minimum 5 years continuous operation, namely 4,3800 hours
- Operating speed range: 1500 rpm – 8500 rpm
- Maximum slide velocity of 130 m/s at bearing outer diameter.
- Lubrication fluid range: 4°C – 80°C
- Pad surface roughness quality of Ra < 0.2 µm (Arithmetic average roughness value)
- Operating pressure up to 1,000 bar
- No limitation on manufacturing sizes, such as is the case for PC

Bearing Design

The design of the ceramic tilting pad thrust bearing (TPTB) derives from proven designs for the MIBG bearings product portfolio. This approach was chosen due to the tight project schedule and the premise of operational reliability that would allow for one to one performance comparison between conventional bearings and the new diamond composite prototype bearing. For the continuation of the development the bearing design will be reassessed taking into account the material properties of the ceramic material to, on one hand further optimize the reliability and robustness of the design, and on the other hand, to reduce the manufacturing costs by pursuing a more material-specific design.

A familiar tilting pad design, selected with offset pivot offers several significant advantages such as operational reliability, a broad experience in calculation / simulation, and verification of similar TPTBs used in a wide range of applications. In addition, PEEK TPTBs of similar design supplied with low viscous lubricant fluids (water or water-glycol) have been tested before (Henssler, Schneider , Gassmann, & Felix, 2015).

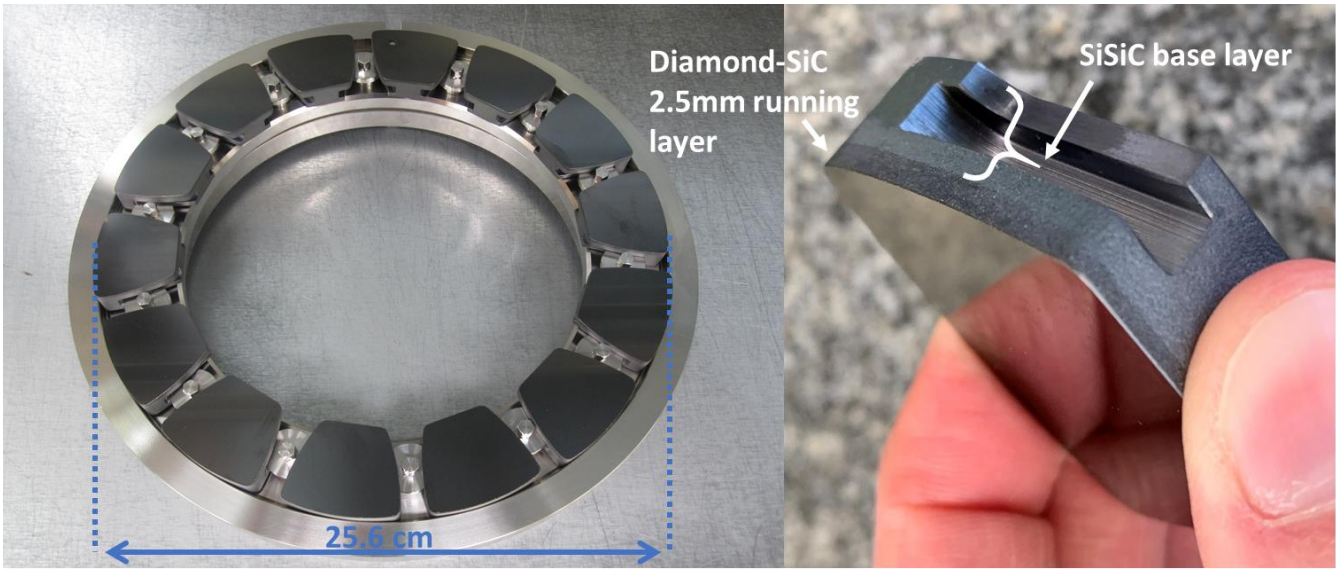

Figure 10: Ceramic layered Diamond-SiC composite tilting pad thrust bearing (14-pads, size 37 mm).

As shown in Figure 11a, an individual pad is a two-layer construction with the running surface layer of Diamond-SiC composite (≈2.5 mm thick) on top of the substrate layer of a conventional reaction bonded SiC material. This design facilitates the implementation of the typical TPTB design since finishing of the radial groove and arcuate grooves (pockets) on the back and sides of the pads did not need be of diamond ceramic.

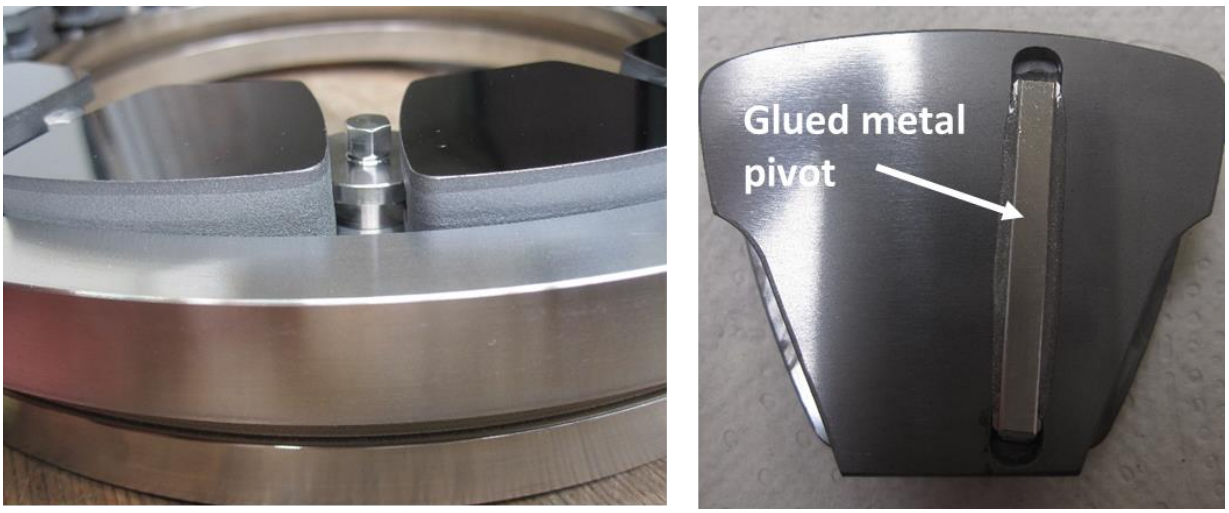

Figure 11: Thrust pads made from graded diamond ceramic material. Base material: Si-SiC -- Top layer: Diamond-SiC (a). Backside of the pad with metallic tilt bar (offset pivot) (b).

As shown in Figure 11b, the metal tilt bar (radial pivot) was glued with a special adhesive into the machined groove. The use of

adhesive bonding for ceramic components has some advantages but must be carefully evaluated in terms of chemical compatibility, stress scenarios, fatigue strength, aging behavior and the process reproducibility. Presently, the authors used an engineered adhesive, cured at 150 °C, and that can maintain the mechanical properties of the joined section of the component up to 250 °C.

The bearing design was selected in line with the existing envelope dimensions of an available test rig. At each rotor speed, calculations determined the specific loads to maintain a lubricant film thickness of at least 7µm. For a lubricant supply temperature of 30 °C and operation at a speed of 6,000 rpm, the calculated maximum bearing unit load equals 62 kN (3.2 MPa). The design as well as the operational safety of this type of TPTB in combination with water as lubricant were already evaluated in past tests with PEEK coated bearings.

The design-related stress pattern on the groove base of the pads was investigated accordingly by means of a FEA (Finite Element Analysis). For this purpose, the maximum operating loads were previously determined by CFD (Computation Fluid Dynamics) delivering the pressure distribution on each pad, which serves as the forces input for the FEA. Figure 12 a) shows the calculated CFD pressure profile on a pad for a bearing load=70kN, and which corresponds to an average (specific) load per pad of 3.6 MPa. For a loading with this pressure profile on the pad, Figure 12b) shows the FEA internal stresses within the pad.

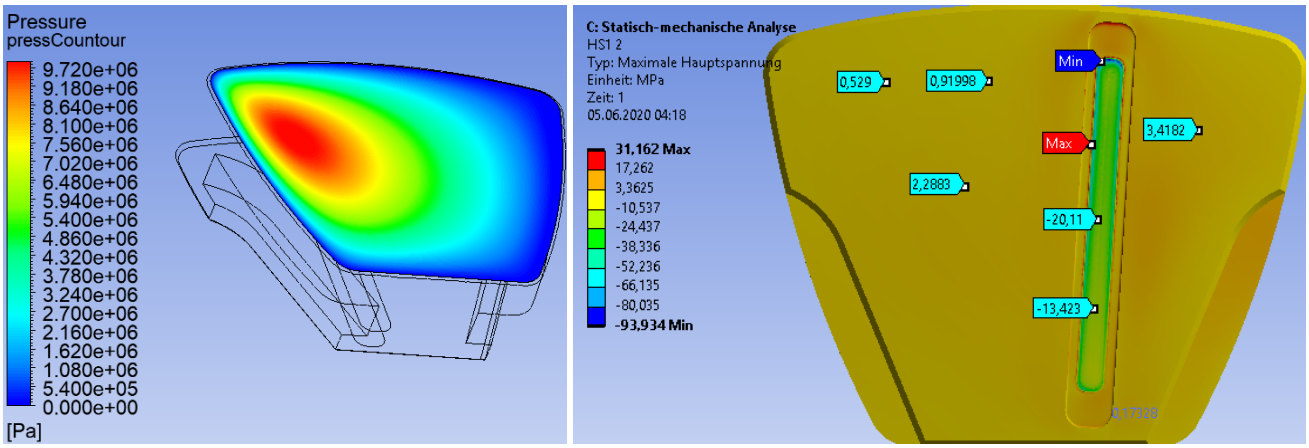

Figure 12: (a) CFD results of pressure (Pa) on a pad, (b) FEA results of the maximum principal stresses (MPa).

As expected, the maximum stresses in the ceramic material occur in the bottom of the groove hosting the pivot. These maximum tensile stresses are the limiting factor for the permissible pad load. The basic groove geometry as well as the dimensions of the tilting bar and the radii at the transition of the groove are decisive to set the level of the calculated principal stresses. Note that a FEA optimization study contemplated a variety of distinct grooves and tilting bar designs toward minimizing the maximum principal stresses. Due to the different failure mechanisms between steel grades and ceramics, one must choose a design that minimizes primarily the tensile stresses.

Subsequently, two pads manufactured with the optimal configuration were subject to destructive testing via a simple test conducted with a hydraulic press exerting a static load on a pad through a clamp (Figure 13a) . For each test, the applied load increased in steps of 2.5 kN up to 35 kN, and later up to 50 kN. After each test a measurement of the pad height was carried out for the determination of invisible cracks or other alterations. No issues were observed up to an applied load of 50kN/pad (unit load = 36.2 MPa). This value is more than 10-times higher than the design load of 62 kN (3.2 MPa) for the whole 14-pad bearing. A significantly large load equaling ~ 88 kN (63.7 MPa) destroyed the pads. Hence, the experiments proved that typical and proven designs for white metal TPTBs are also suitable for TPTBs with ceramic pad materials.

Figure 13: (a) pad and clamp, (b) load application on pad with a hydraulic press.

Thrust bearing design

Within the scope of this work, it was necessary to modify the thrust collar with a new design suitable for ceramics. The design was adapted to achieve lower stress amplitudes when applying loads during operation. Therefore, the original design of the inner contour of the ceramic ring was changed from a sharp edge to a softer, rounded transition of the two semicircles to the straight wall sections, as shown in Figure 14.

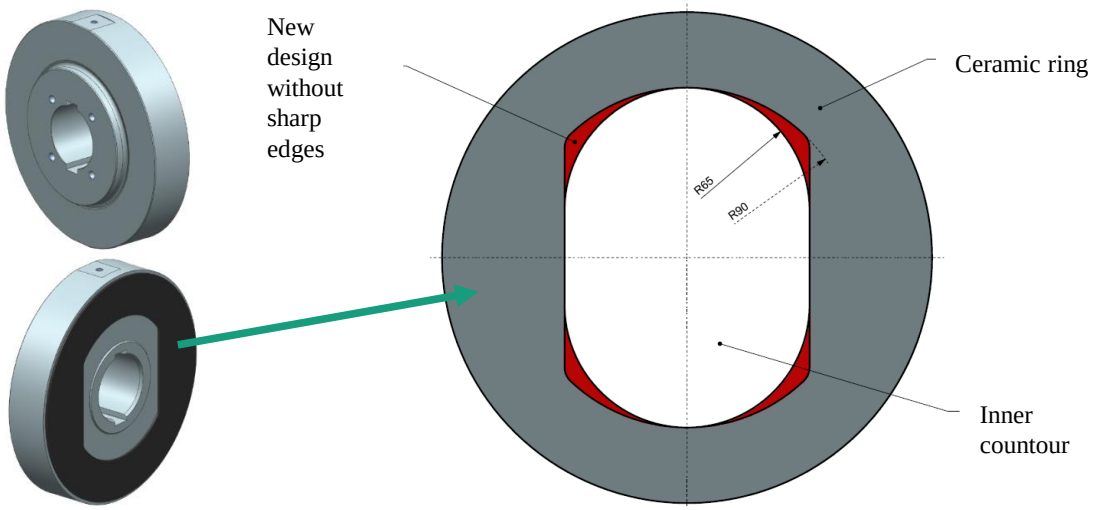

Figure 14: Thrust collar ceramic design improvement with rounded transitions.

This design improvement was done to reduce the internal stresses within the ceramic disk which occur due to differences in thermal expansion coefficient of material of the ceramic disk and the metal carrier.

Step	1st	2nd	3rd	4th
Grain diameter	D 126 µm	20 µm ≤ D ≤ 40 µm	14 µm ≤ D ≤ 20 µm	3 µm ≤ D ≤ 6 µm
Machining time	360 min	180 min	180 min	180 min

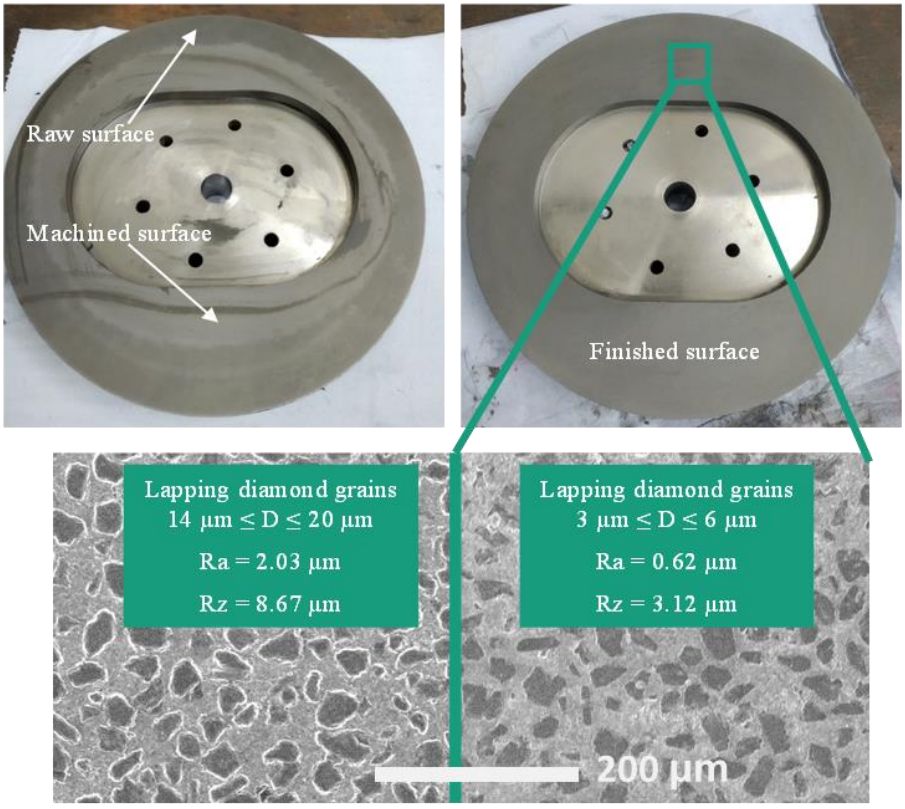

Figure 15: Machining strategy for lapping and 3D profile of machined surface of the Diamond-SiC composite

As stated earlier, when compared to metallic materials, the use of novel Diamond-SiC composite can offer numerous advantages, e.g. components with low wear rate and a long lifetime. With regard to the manufacturing of components made of Diamond-SiC- composite, requirements such as high dimensional accuracy and surface quality can only be achieved with post-processing after the sintering. The machining of Diamond-SiC composites is quite demanding due to its mechanical properties, and which leads to a high wear of the machining tool and requires the use of diamond abrasive grains. Moreover, in contrast to the machining of monolithic ceramics, there is hardly any scientific literature on the machining of Diamond-SiC composites; hence it remains a challenge in terms of resultant surface characteristics, tribological properties, geometric accuracy and process costs.

One of the most significant technologies for machining Diamond-SiC composites is a lapping processes with diamond abrasives. Although extremely high wear of the abrasive lapping tools is expected during machining, it can be reduced by using optimized machining parameters, strategies and tools. To achieve plane-parallel faces, both sides of the Diamond-SiC ring were machined via one sided lapping. The oil-grain-suspensions used in the process are a 1:1 composition of diamond grains (D126, D40, D20, D6) and lapping-oil. The workpiece was only loaded with 20 kg, which corresponds to a specific surface load of approx. 61 g/cm2. As shown in Figure 15, the machined surface has a lighter shade of grey than the rough surface, and thus the machining progress can be monitored by checking the growth of the light grey area. The very high hardness of the Diamond-SiC surface requires rather frequent dressing of the cast iron lapping disk, hence adding a lot of set-up time to the process. Once the surface is planed with D126-suspension, the more fine-grained suspensions are used successively to reduce the overall surface roughness. After a cumulative process time of twelve hours, an arithmetic average roughness value of Ra = 0.62 µm is achieved.

After the machining process, the Diamond-SiC ring was bonded to a special steel base body. With the final Diamond-SiC composite ring thickness considered, the mounting pocket in the steel body was machined, with six supports, to ensure proper gap size for the gluing process (0.88 mm) and overall part thickness.

Figure 16: Thrust collar assembly process

As shown in Figure 16, prior to the application of the adhesive, the mounting pocket surface was sand blasted to increase surface roughness and therefore adhesion. The adhesive used to join the ceramic ring and the steel body was a heat activated glue. The adhesive is the same adhesive which has been used for the gluing of the metal pivot to the tilting pad. It is an engineered adhesive, which has been cured at 150 °C. Once cured, it maintains the mechanical properties of the joint up to 250°C. To keep thermal- and residual stresses to a minimum, the parts are slowly heated to 150 °C, and later cooled over a period of 10 hours. The gluing process is termed successful, as the cooled down part showed no cracks in the ceramic ring or any other distortions.

After the bonding process, the Diamond-SiC surface becomes a reference for finishing the steel base body via turning. The most time-consuming and demanding process in the manufacturing of the novel thrust collar was the planar lapping of the Diamond-SiC ring and the excessive amount of dressing required to keep the cast iron lapping discs flat. The use of large diamond grains (D126) is unusual in polishing. However, this was a developed method to first correct the shape of the Diamond-SiC ring. The improvement of the surface quality was feasible through the use of smaller diamond lapping grits. By using different diamond grit sizes at different steps of the lapping process, it was possible to produce a thrust collar with the required surface quality and precision.

RESULTS FROM TILTING PAD THRUST BEARING TEST

Test set-up

Figure 17 depicts a component qualification test rig for thrust bearings and that uses a variety of clean fluids as lubricant. An external circulation pump gives full flexibility to adjust the lubricant flow rate supplied to the test bearing. The rig was used for several prior qualification programs (Henssler, Schneider , Gassmann, & Felix, 2015).

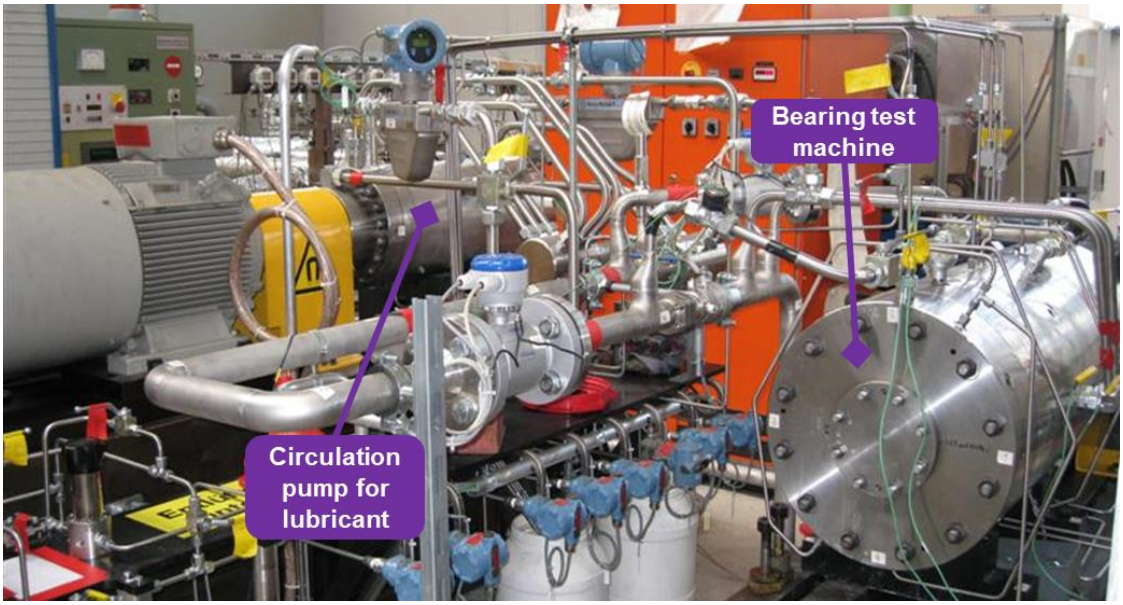

Figure 17: Component qualification test rig for product lubricated thrust bearings

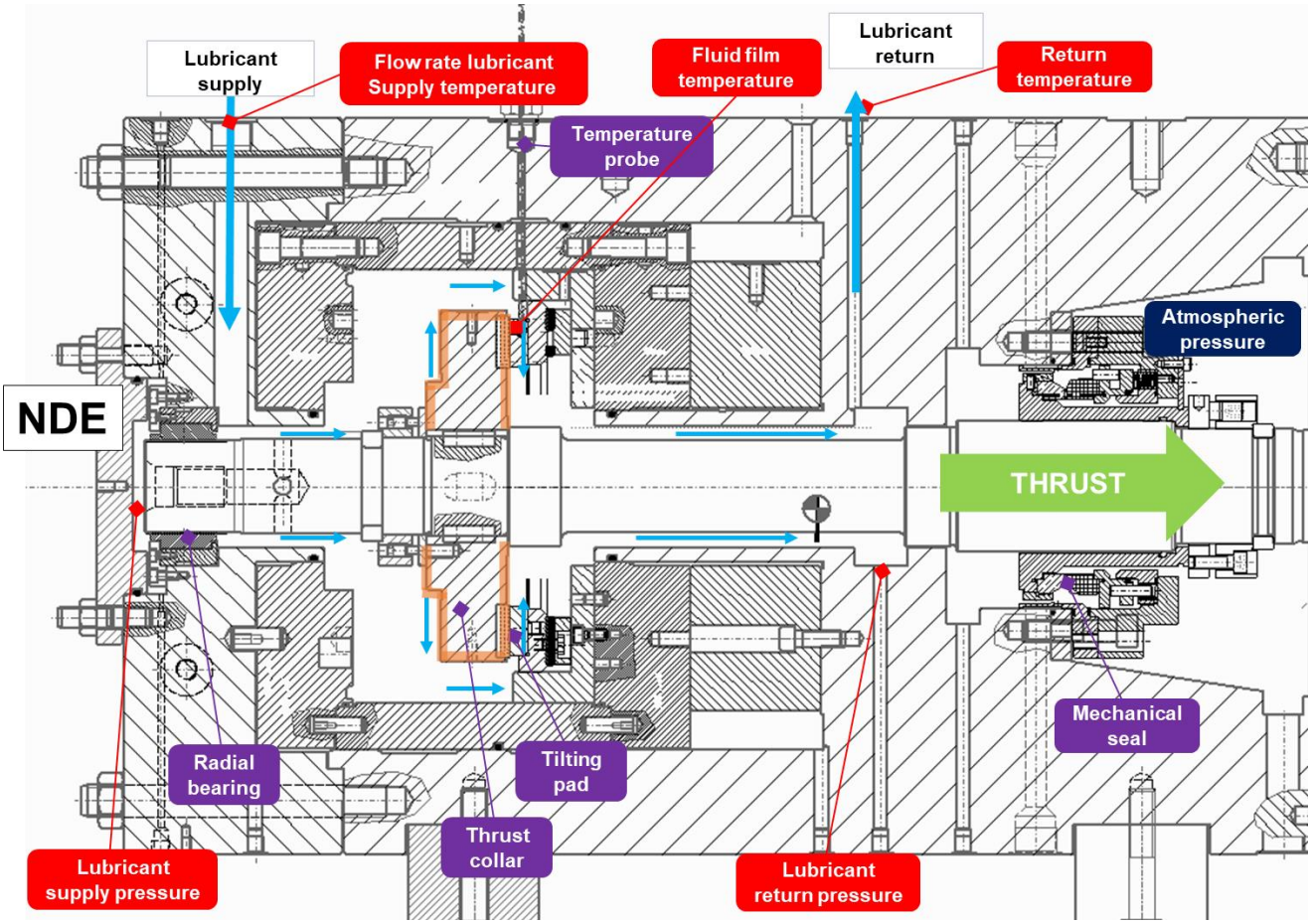

Figure 18: Cross sectional view of thrust bearing test rig, indicating the position of the various sensors.

The instrumentation as per Figure 18 allows the measurement of the fluid film temperature of the loaded bearing, the applied load, the lubricant flow and an estimation of the drag power loss from a thermal energy balance across the bearing. The supply and return temperature of the lubricant together with its flow rate allow the determination of the heat generated in the test rig. This signal is then corrected by the known drag power loss of the rotating shaft. The thrust load is controlled by regulating the pressure difference across the externally-pressurized mechanical seal. The externally-pressurized mechanical seal acts thus as balancing disc. The difference pressure across the mechanical is regulated by regulating the pressure of the lubrication fluid, which is done with a HPU (hydraulic power unit). The lubrication fluid is in a close loop and gets circulated by a circulation pump. Unfortunately this test rig doesn't have proximity probes to measure the axial displacement of the thrust collar for the direct measurement of the fluid film thickness. The fluid film thickness has thus to be calculated with CFD. The bearing characteristic dimensions and operating configuration are:

- Bearing pad surface: 19,353 mm^2
- Pad inner and outer diameter: 182.1 mm and 256.1 mm
- Composite material (Diamond-SiC) tilting pads with metallic pivot shoes; offset pivot 60%
- Lubrication: flooded design

Test results

The bearings were tested to evaluate the robustness and to confirm their improved performance due to the novel material superior mechanical properties. The operating conditions are

- Shaft speed range from 1,500 rpm to 6,000 rpm (maximum surface speed of 80 m/s)
- Lubricant fluid temperature range: 20 °C to 60 °C
- Bearing load corresponding to film thicknesses down to 7.5 µm (fluid film thicknesses calculated with CFD for given load)
- Untreated tap water as the lubricant fluid

Figure 19 gives an overview of the test campaign. The bearings operated for over 36 h at a variety loads and shaft speeds.

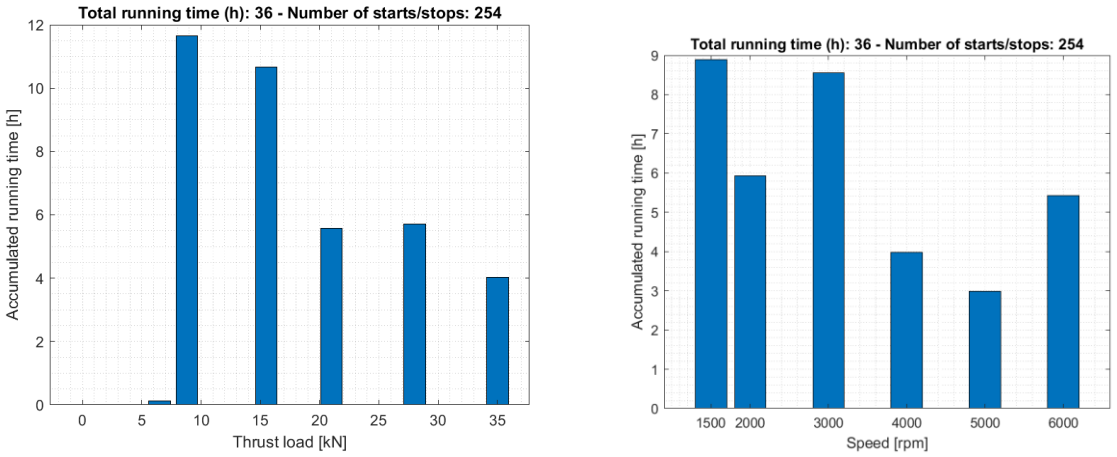

Figure 19: (a) Test campaign overview; accumulated operating time at various thrust loads, and (b) Accumulated operating time at various shaft speeds.

As known before, the most critical conditions for the TPTB is during start-up. Over 250 start and stops were performed at a variety of thrust loads at start-up. The shaft torque is measured by the VFD (variable frequency drive) of the motor (corrected with the gear ratio of the gearbox). As can be seen in Figure 20, the start-up torque, also called break-away torque, depends on the bearing load. A start-up under load is more demanding and challenging for the bearing. For a load of 15 kN (0.78 MPa), an average start-up torque of 50 Nm was registered along with a peak (max.) start-up torque of 70 Nm. For a thrust load of 10 kN (0.5 MPa), an average start-up torque of 30 Nm and a peak start-up torque of 42 Nm were recorded. The peak shaft torque has to overcome the friction torques of the other components as well, such as the radial bearings and the mechanical seal. It assumed that the majority of the torque is needed to overcome the friction forces of the thrust bearing, since the thrust bearing is highly loaded and has a larger diameter than the other components.

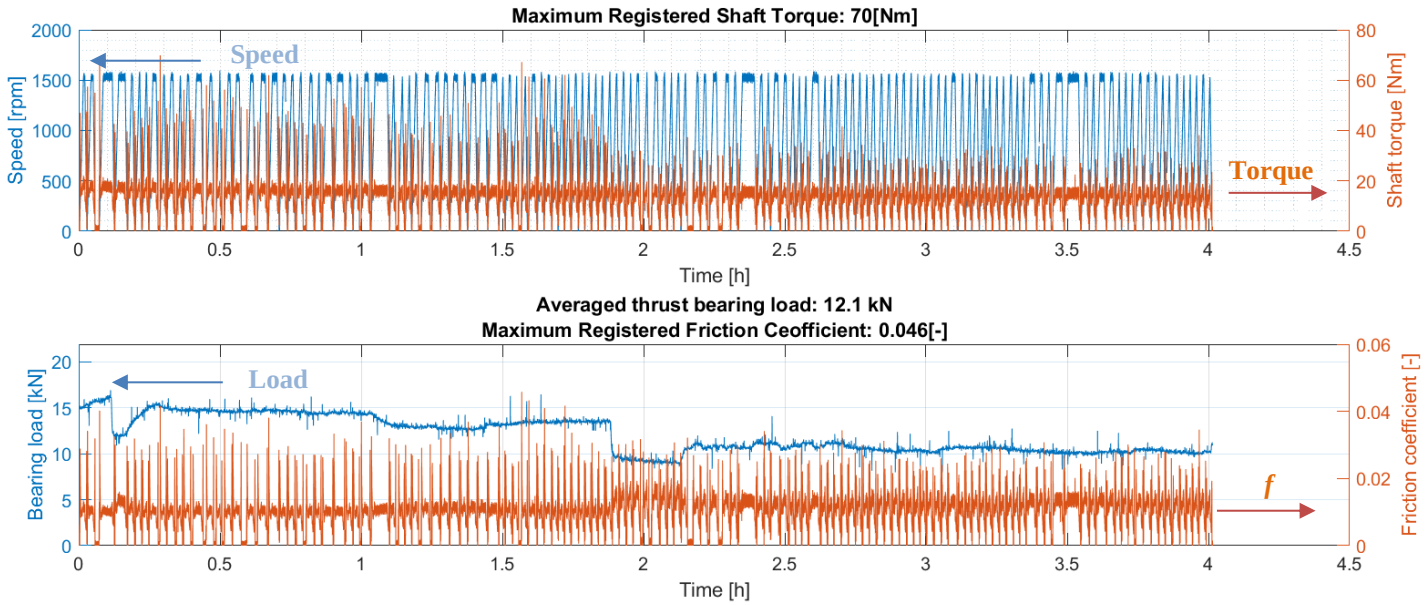

Figure 20: Intermittent shaft start-up and stop tests under various thrust loads: rotor speed, drag torque, load and friction coefficient vs. time.

A dry-friction coefficient (f) equals

$$Dry\ friction\ coefficient = f = \frac{Shaft\ torque}{Thrust\ bearing\ load * average\ thrust\ bearing\ radius}$$

The measured peak friction coefficient during start-up is f=0.046, similar to the f measured during the tribological material tests. The result demonstrates that thanks to the very low f, an exceptionally low break-away torque is apparent. This means that the pads will be exposed to smaller forces during start-up. As seen in Figure 21, the peak torque and friction coefficient occur during the initial start-up moments of shaft acceleration from rest; that is, during the breaking loose of the rotor. The friction coefficient as the shaft speed crosses a certain threshold magnitude, which corresponds to the establishment of the fluid film; and thus the bearing lift off. The reverse occurs during shaft deceleration from its top speed.

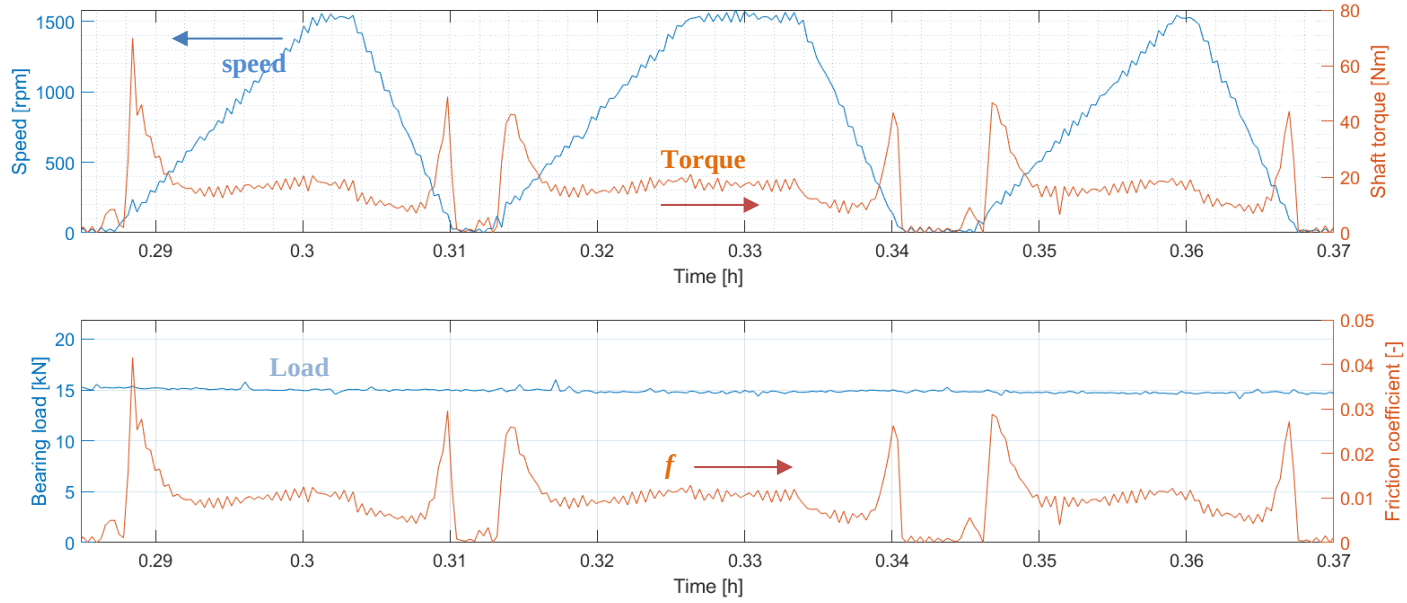

Figure 21: Zoom on three consecutive start and stop cycles: rotor speed, drag torque, load and friction coefficient (f) vs. time.

Figure 22 shows the results of a test conducted at 6,000 rpm (surface speed of 80 m/s) and with clean water supplied at 55 °C. The water heats due to the mechanical and hydraulic losses within the closed loop and reaches 55°C after 1 hour of running time. The test is performed at an average thrust load of 31.4 kN (1.62 MPa), which corresponds to a calculated minimum fluid film thickness of 9 µm. The bearing losses are calculated from the measurement of the temperature rise of the lubrication fluid flowing through the bearing. The bearing torque is derived from these calculated bearing losses. The shaft torque is measured by the VFD. The shaft power (=test rig losses) is derived from the shaft torque.

The average torque of the bearing assembly (orange area in Figure 18) is 73 Nm, which means that the average friction coefficient is at most f=0.021. The viscous wall friction (i.e. skin friction or also called windage losses) between the fluid and the rotating surface of the thrust collar is included in the (torque) measurement. The actual friction coefficient of the lubricated bearing will thus be significantly lower once it lifts and operates under a hydrodynamic fluid-film lubrication regime. To measure the actual friction coefficient of the fluid film bearing alone, a direct measurement of the torque on the pad carrier would be needed.

Due to the low friction coefficient of the material and the low viscosity of the lubricant, a relatively low temperature rise is recorded in the fluid film. Significantly higher fluid temperature rises were measured for a conventional PEEK thrust bearing evaluated in the same test machine (Henssler, Schneider , Gassmann, & Felix, 2015) and supplied with a water-glycol mixture. The total bearing power losses consist of the losses of the entire bearing assembly, namely the losses in the fluid film as well as the disk friction losses of the rotating thrust collar (the area indicated in orange in Figure 18).

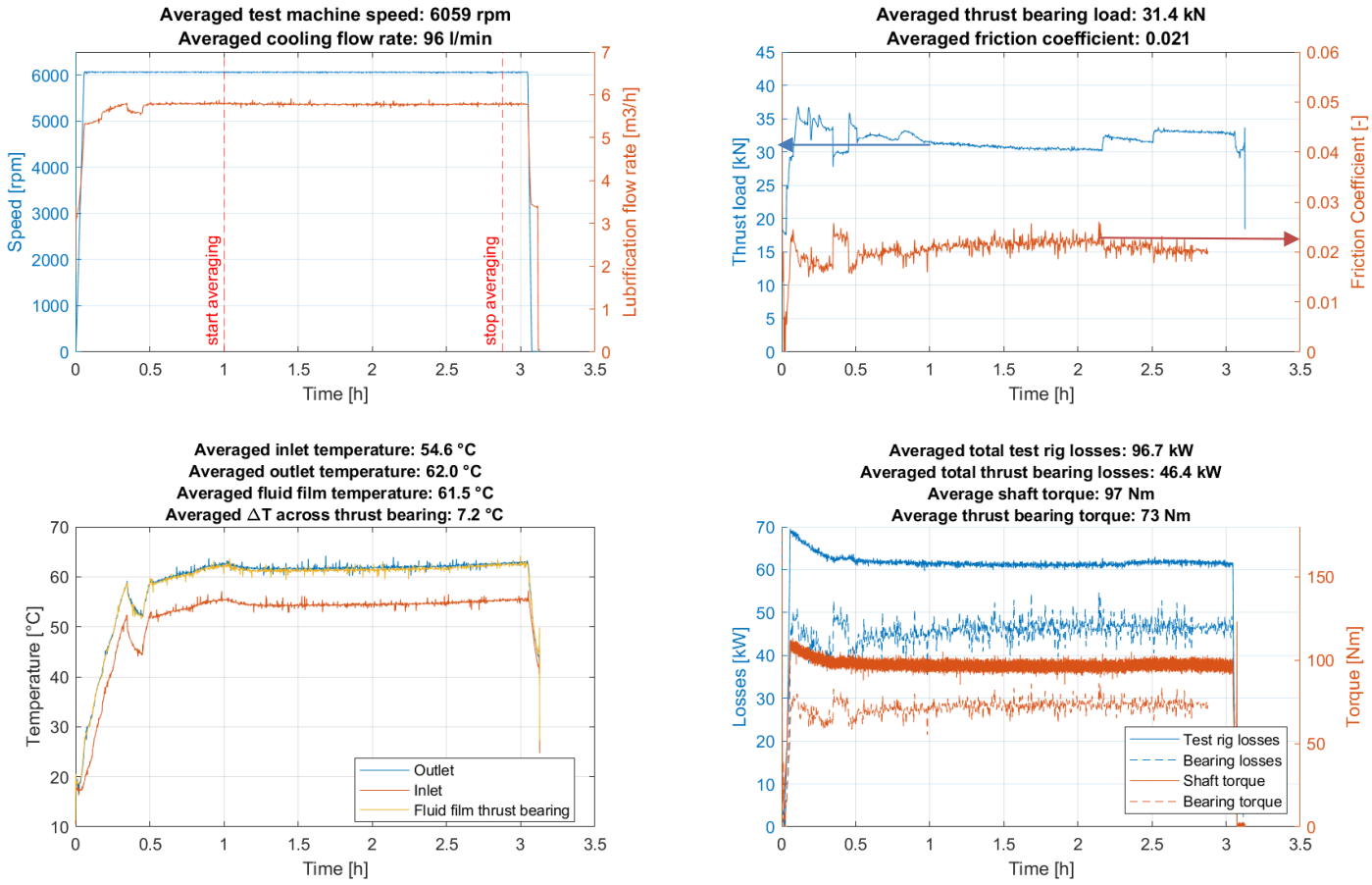

Figure 22: results of test performed at 6,000 rpm and 55 °C supply water temperature - graph (a) speed and lubricant flow rate vs time, (b) thrust load and friction coefficient vs time, (c) lubricant temperature at inlet, outlet and in the fluid film vs time, (d) Test rig and bearing losses and torque vs time.

Post-test condition of bearing components
As seen in the photographs in Figure 23, the components of the thrust bearing remained as in as-new condition after completion of the tests.

Figure 23: Post-test condition of the pads and thrust collar in ceramic TPTB after a 36 hour test campaign.

Detailed analysis of the pad surface after the qualification test
After the performance test in the test rig described above, the condition of one of the Diamond-SiC ceramic pads is further evaluated with some detail. The overall appearance of the slide pads can be assessed as very good, no chipping or break out is visible. However, all pads show one area which looks more polished than the rest of the surface. Apparently, this is the contact area of the pad with the thrust collar. Figure 24 shows the optical appearance of the pad and a stitched picture taken by a high-resolution 3D microscope. The areas marked with A, B and C denote distinct areas: A is outside of the contact area, B is within the area of highest grading, and C is in the area with intermediate grading. B and C are within the contact area at the moment of start-up and which is also the area with the lowest fluid film thickness during normal operation. Furthermore, a slight waviness of the pad surface, with an amplitude of less than 0.5 µm (0.0005 mm), outside of the contact area is visible, and which is attributed to the grinding process of the pad.
The green lines in the polished area, shouldn't be considered, as they are an artefact of the stitching process of the picture, composed of a multitude of smaller pictures.

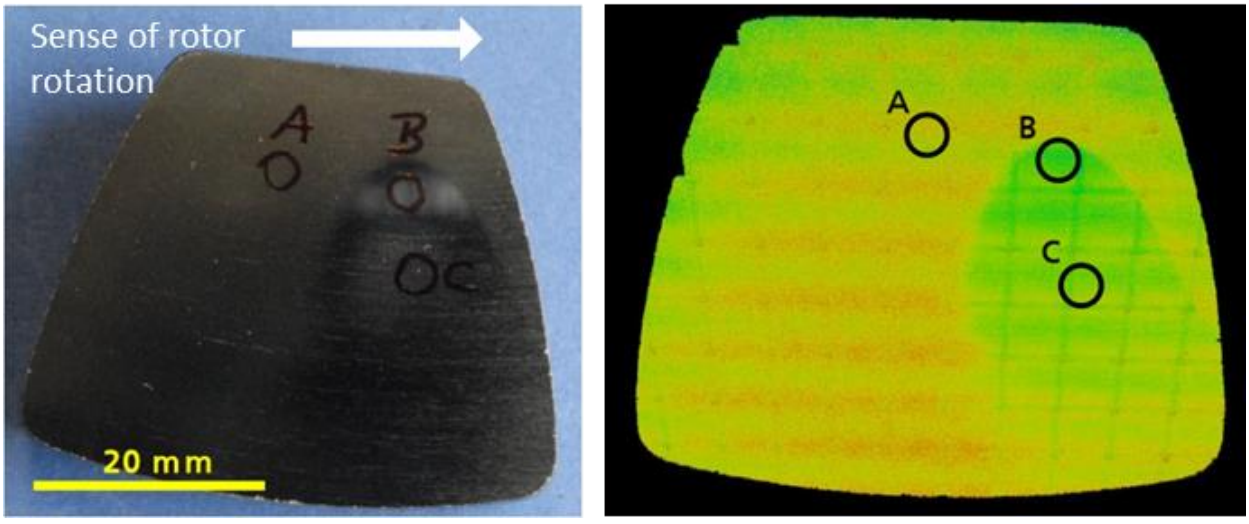

Figure 24: Photographs (a) stitched picture (b) taken by a high-resolution 3D microscope of pad No. 6 after performance tests. (reddish color corresponds to a higher surface roughness and green color corresponds to a lower surface roughness)

The areas marked A, B and C were examined in detail to determine the wear of the sliding pad during the performance test. Figure 25 shows the 3D profiles of areas A and B. The peak roughness of area A is approximately 350 nm (0.35 µm), whereas area B shows a

smoother surface with a roughness in the range of 150 nm (0.15 µm). The results of area C were slightly above the magnitude\s of area B, indicating less contact during the test.

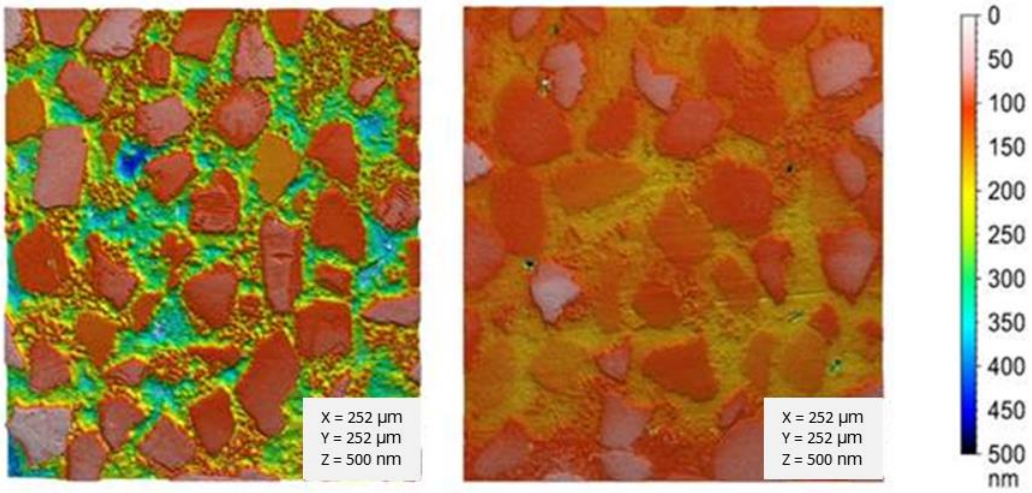

Figure 25: 3D profiles of area A (left) and area B (right) with adjusted height scale.

It could be concluded that the performance test led to a smoothing of the pads' surfaces. Obviously, the diamond grains, which were already flattened by the grinding process during manufacturing of the pads, were further smoothed while in contact with the thrust collar, made from the same material. The fact that no break-out of diamond particles can be observed, shows the good bonding between the diamond particles and the SiC matrix. Note that 250 start-up and stop events were performed with a significant thrust load applied from the start. This means that the bearing will have operated under serious boundary lubrication conditions during the first moments of each start-up. This resulted in an additional polishing of the material in the contact area. A wear of approximately 200 nm was measured in this contact area.

Keeping in mind that the only occurrence of wear is expected during the start-up and stop events, the wear rate is exceptionally low. Furthermore, it must be considered, that a flattening of the diamond grains increases the percentage contact area, which may lead to a further reduction of the wear rate.

CONCLUSIONS

A novel ceramic material, namely Diamond-SiC composite material, was tested to assess its suitability as running material for product lubricated bearings. In comparison to its peers, the tribological tests show that the material exhibits excellent erosion and wear characteristics. It is shown that the material has a low friction coefficient which remains very steady under periodic dry running conditions.

The manufacture of the prototype bearing also validated the feasibility of the manufacturing and assembly processes as well as the material treatment processes. With the manufacturing of the 256 mm ceramic thrust disk, it is shown that large single-pieces can be manufactured within tolerance.

The bearing running tests demonstrated that due to the superior material properties, the bearing excelled in its performance. Very low break-away torques were measured during start-up conditions, i.e., a small friction coefficient during the boundary lubrication conditions which occur during the first seconds of each start-up and under high thrust loads (1.13 MPa). A polishing of less than 1 nm per start-up was measured, i.e., a negligible amount. This shows the bearing can easily handle start-up conditions under large thrust loads. The bearing is thus expected to have a MTBM of at least 43,800 hours (five years of continuous operation).

A low temperature rise in the lubricant (clean water) and a small temperature difference between the fluid film temperature and the outlet temperature was measured. The high thermal conductivity and low friction coefficient of the novel material produced these results. Related to this, also a very low drag power dissipation was confirmed through measurements. After a 36 hours test campaign with 250 start-up and stops under a significant load, the bearing came out as new, and which validates the robustness and reliability of the design.

The next important step in the bearing development and qualification program is to test the bearing as lubricated with a sand loaded lubricant. The excellent abrasion resistance of the material has already been tested and validated through several material tribological tests. The design of the bearing assembly will be further improved in order to increase its reliability while operating with a sand loaded lubrication fluids The design improvement will consist of minimizing the risk of stagnant fluid zones and hence sand accumulation within the bearing assembly, and which can result in a restriction of the free movement of the tilting pads.

The current bearing design will also be further improved towards a more ceramic-friendly bearing design (e.g. to reduce the tensile

stresses at the interface with the metallic pivot in the prototype bearing and at the interface of the ceramic ring to the metal body in the thrust collar). The final objective of this development is to enable the commercialization of this novel bearing technology and coupled to the product development of reliable topside and subsea product lubricated water injection pumps.

NOMENCLATURE

API = American Petroleum Institute
ASTM = American Society for Testing Materials
CVD = Chemical Vapor Deposition
CNC = Computer numerical control
CFD = Computational Fluid Dynamics
CAPEX = Capital Expenditure
FEA = Finite Element Analysis
HPU = Hydraulic Power(/Pressure) Unit
JIP = Joint Industry Project
MIBG = Miba Industrial Bearings, Germany
MTBM = Mean Time Between Maintenance
OPEX = Operating Expenditures
PCD = Polycrystalline Diamond
PEEK = Polyether Ether Ketone
PLB = Product Lubricated Bearing
PCD = Polycrystalline Diamond
PEEK = Polyether Ether Ketone
PLB = Product Lubricated Bearing
Ra = Arithmetic average roughness value (L)
Rz = Peak-to-peak roughness value (L)
SiC = Silicon Carbide
Si-SiC = Silicon infiltrated Silicon Carbide
SSiC = Solid phase sintered Silicon Carbide
SRU = Sulfate Removal Unit
TPTB = Tilting Pad Thrust Bearing
UTA = Umbilical Termination Assembly
VFD = Variable Frequency Drive

REFERENCES

Bernhard, G., Droescher, P., Gassmann, S., & Inforsati, M. (2016). High Pressure, High Temperature Shaft Seal For A Multiphase Subsea Pump. 45th TurboMachinery & 32nd Pump Symposia. Houston: Texas A&M. doi:10.21423/R11S3N

Bourne, M., Felix, T., De Raeve, K., & Gassmann, S. (2019). Patent No. EP3808984A1.

Eriksen, S., Bruun, H., Larsen, S., & Hollingsaeter, T. (2013). Patent No. WO2014206919A1.

Henssler, D., Schneider , L., Gassmann, S., & Felix, T. (2015). Qualification And Optimization Of Solid Polymer Tilting Pad Bearings For Subsea Pump Applications. 44th Turbomachinery & 31st Pump Symposia. Houston: Texas A&M. doi:10.21423/R14329

Herrmann, M., Kluge, E., Rödel, C., McKie, A., & van Staden, F. (2014). Corrosion behaviour of silicon carbide-diamond composite materials in aqueous solutions. Journal of the European Ceramic Society, 34(10), 3362-3371.

Lindøen-Kjellnes, H. (2021). Subsea Water Injection - Potential Savings on Economic and CO2 Footprint. Underwater Technology Conference. Bergen: UTF.

Matthey, B., Kunze, S., Hörner, M., Blug, B., van Geldern, M., Michaelis, A., & Herrmann, M. (2017). SiC-bonded diamond materials produced by pressureless silicon infiltration. Journal of Materials Research, 32(17), 3362-3371.

Presser, V., Krummhauer, O., Nickel, K., Kailer, A., Berthold, C., & Raisch, C. (2009). Tribological and hydrothermal behaviour of silicon carbide under water lubrication. Wear 266, 771-781.

Swann, M., Watkins, J., & Bornstein, K. (1997). Present limits of operation of product lubricated and magnetic bearings in pumps. 14th Internationl Pump Users Symposion (pp. 113-128). Houston: Texas A&M. doi:10.21423/R1MX2X

Üre Villoria, M., & Welschinger, T. (2014). Water injection pumps for the oil industry: pushing the boundaries of centrifugal pump design. Sulzer Technical Review, 1.

ACKNOWLEDGEMENTS

A special *thank you* goes to Simon Gassmann, Thomas Welschinger, Benedikt Trottmann and Marcelo Inforsati for their active contribution to this technology development and for sharing their knowledge and vast experience.

The authors would like to thank Prof. Luis San Andrés for reviewing and editing the lecture.

The authors are also grateful to their Companies for the permission to publish this information and contribute to the knowledge sharing in the rotordynamics technical community.

The authors thank the German government for the funding package provided to the Joint Industry Project (JIP), namely the SubseaSlide JIP. This JIP has been set-up for the optimization and industrialization of the thrust bearing & thrust collar and also the development of journal bearings and the testing of these bearings on a newly developed sand test loop. The JIP has been started in September 2020 and is expected to last for 3 years.